Search for Heavy Neutral Leptons with IceCube DeepCore

Dissertation
zur Erlangung des akademischen Grades
doctor rerum naturalium
(Dr. rer. nat.)

im Fach: Physik
Spezialisierung: Experimentalphysik

eingereicht an der
Mathematisch-Naturwissenschaftlichen Fakultät
der Humboldt-Universität zu Berlin

von
Leander Fischer M. Sc.
geboren am 24. Oktober 1992
in Heidelberg

Präsidentin der Humboldt-Universität zu Berlin
Prof. Dr. Julia von Blumenthal

Dekanin der Mathematisch-Naturwissenschaftlichen Fakultät
Prof. Dr. Caren Tischendorf

Colophon

This document was typeset with the help of KOMA-Script and LaTeX using the open-source kaobook template class.

The source code of this thesis is available at:
https://github.com/LeanderFischer/phd_thesis

Zusammenfassung

Zusammenfassung . . .

Abstract

Abstract . . .

Todo list

Contents

List of Figures

List of Tables

Introduction | 1

The neutrino was postulated by Wolfgang Pauli [1] in 1930 to explain the continuous energy spectrum of electrons originating from beta decay. Cowan and Reines confirmed this prediction of a light, neutral particle in 1956 when they discovered the electron neutrino using inverse beta decay [2]. Two additional neutrino flavors were found in the following years, and with the discovery of the muon neutrino in 1962 [3] and the tau neutrino in 2001 [4], the current theory of neutrinos in the standard model (SM) was established.

Although neutrinos were first believed to be massless, experimental evidence showing the existence of mixed neutrino states started to appear in the 1960s [5]. Mixing between different physical representations of neutrinos is proof for differences in their masses. The resulting phenomenon of neutrino oscillations can be incorporated into the standard model by extending it to include massive neutrinos. How massive they are and how strong is the mixing between neutrino states has to be obtained from measurement. Today there are a variety of precision oscillation experiments using solar, reactor and atmospheric neutrinos to tighten the constraints on the neutrino oscillation parameters. IceCube is one of those leading experiments probing the oscillation theory with atmospheric neutrinos.

The IceCube Neutrino Observatory [6] was constructed between 2004 and 2010 at the geographic South Pole. It is the first cubic kilometer Cherenkov neutrino detector and consists of 5160 optical sensors attached to 86 strings, drilled down to a maximum depth of $\sim 2500\,\mathrm{m}$ into the Antarctic ice. Neutrinos are detected by the Cherenkov light that is emitted by secondary particles produced in neutrino-nucleon scattering interactions in the ice. With DeepCore, a more densely instrumented sub-array of IceCube, the neutrino detection energy threshold can be lowered to approximately $5\,\mathrm{GeV}$.

At these energies, the similarity in event signatures poses difficulties in identifying different neutrino flavor interactions. Muon neutrino charged-current interactions produce light tracks as opposed to charged-current interactions of electron and tau neutrinos as well as neutral-current interactions of all neutrinos that produce light cascades. The sparse instrumentation of IceCube makes it more challenging to separate track- and cascade-like events. In this thesis, a novel method to distinguish those two event types is developed. In contrast to previously used univariate separation techniques, the multivariate machine learning method applied here maximizes the use of information from the detector response. Through the use of a Gradient Tree Boosting algorithm the separation of events in track and cascade is improved. As a result of the improved separation, the uncertainty to the atmospheric neutrino oscillation parameters Δm_{32}^2 and θ_{23} is significantly reduced.

This thesis is structured as follows.

(Re-)write introduction for PhD thesis (just copy paste from M.Sc.).

[1]: Pauli (1978), *Dear radioactive ladies and gentlemen*

[2]: Cowan et al. (1956), *Detection of the Free Neutrino: a Confirmation*

[3]: Danby et al. (1962), *Observation of High-Energy Neutrino Reactions and the Existence of Two Kinds of Neutrinos*

[4]: Kodama et al. (2001), *Observation of tau neutrino interactions*

[5]: Davis et al. (1972), *Proceedings of the Neutrino '72 Europhysics Conference*

[6]: Aartsen et al. (2017), *The IceCube Neutrino Observatory: instrumentation and online systems*

Standard Model Neutrinos | 2

This chapter introduces the basic properties of neutrinos, their place in the Standard Model of particle physics (SM) and their peculiarities following the description of [7].

2.1 Standard Model Particles

2.1.1 Electroweak Symmetry Breaking

2.1.2 Charged Fermion Masses

2.1.3 Neutrino Masses

Dirac

Majorana

2.1.4 See-Saw Mechanisms

2.1.5 Radiative Neutrino Masses

2.2 Neutrino Properties

2.2.1 Quantum Numbers

2.2.2 Mass

2.2.3 Active Neutrino Flavors

2.3 Neutrino Interactions

2.3.1 Weak Interactions after Symmetry-Breaking

The neutrino is an elementary particle in the SM [7]. It belongs to the class of leptons, which itself is a subclass of elementary fermions (spin $\frac{1}{2}$ particles). The fermions - six quarks and six leptons - form the matter content of the universe. Quarks take part in all three interaction types (forces) of the SM: strong, weak, and electromagnetic (EM) [8]. The charged leptons - electron, muon, and tau - are subject to the weak and the EM interaction. Neutrinos carry neither electric charge nor color charge and therefore only take part in weak interactions. There are three distinct neutrino flavors - electron neutrinos, muon neutrinos and tau neutrinos (ν_e, ν_μ, and ν_τ) [9] - each corresponding to their charged lepton counterparts.

(Re-)write SM neutrino chapter for PhD thesis (just copy paste from M.Sc.).

[7]: Thomson (2013), *Modern particle physics*

[8]: Glashow (1961), *Partial-symmetries of weak interactions*

[9]: Tanabashi et al. (2018), *Review of Particle Physics*

[7]: Thomson (2013), *Modern particle physics*
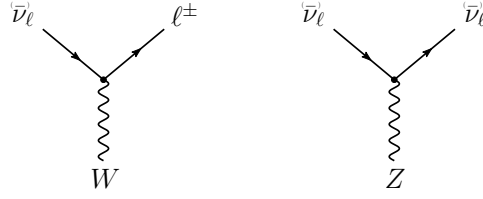
Figure 2.1: Feynman diagrams of charged-current (left) and neutral-current (right) neutrino weak interactions. Taken from [10].

In the SM, weak interactions are mediated by the three massive bosons $\mathbf{W^+}$, $\mathbf{W^-}$, and $\mathbf{Z^0}$ [7]. The large boson masses ($m_{\mathbf{W}} \sim 80\,\text{GeV}$, $m_{\mathbf{Z}} \sim 90\,\text{GeV}$) result in a short range of the force of about 10^{-18} m. Weak interactions carried by $\mathbf{W^\pm}$ bosons are called charged-current (CC) interactions, because charge is transferred between the interacting particles. In CC interactions, a neutrino is converted into its corresponding charged lepton or vice versa. Neutral current (NC) interactions are those mediated by $\mathbf{Z^0}$ bosons. Here no charge is transferred. The Feynman diagrams for CC and NC interactions are shown in Figure Figure 2.1.

Although neutrinos are massless in the SM, we know today that they do have a small mass. The observed phenomenon of neutrino oscillations (see Section Section 3.1) is based on the fact that there is a mass difference between the three neutrino mass eigenstates. From neutrino oscillation measurements the absolute mass scale cannot be determined, since they only depend on the mass differences, but there are upper limits on the sum of all neutrino masses from cosmological observations. These upper limits are typically between 0.3 and 1.3 eV [9].

[9]: Tanabashi et al. (2018), *Review of Particle Physics*

2.3.2 Neutrino-Lepton Scattering

Particle-Antiparticle Scattering

2.3.3 Neutrino Interactions with Nuclei

To describe the neutrino detection principle of IceCube explained in Chapter Chapter 4 we need to understand the weak interaction processes that occur at the energies relevant for this work ($10 - 100\,\text{GeV}$). The cross-sections are dominated by the following neutrino-nucleon interactions: quasi-elastic scattering (QE), resonant scattering (RES), and deep inelastic scattering (DIS). The relative importance of the different processes depends on energy as can be seen in Figure Figure 2.2.
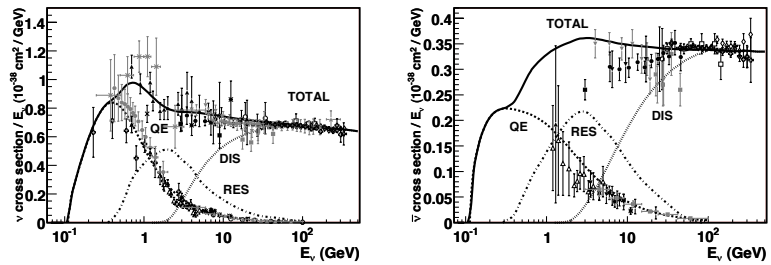
Figure 2.2: Total neutrino(left) and antineutrino(right) per nucleon cross-section divided by neutrino energy plotted against energy. The three main scattering processes quasi-elastic scattering (QE), resonant scattering (RES), and deep-inelastic scattering (DIS) are depicted. Taken from [11].

[11]: Formaggio et al. (2012), *From eV to EeV: Neutrino cross sections across energy scales*

An extensive description of all the interactions and the differences between neutrino and antineutrino cross-sections can be found in [11]. At energies below $5\,\text{GeV}$, QE and RES occur and the neutrinos interact

with approximately point-like protons and neutrons. The cross-sections of these processes are not linear in energy and the transition region to higher energies is poorly understood. At higher energies, the interactions are dominated solely by DIS which has a linear dependence on energy above $\sim 20\,\text{GeV}$. For a given neutrino energy, it is possible to predict the cross-section in this region. Here neutrinos interact with a single quark, breaking apart the nucleus and producing a shower of relativistic secondary particles. Neutrino DIS is the primary detection channel of IceCube. From Figure Figure 2.2 it can be seen that the interaction cross-sections are very small of the order of $10^{-38}\,\text{cm}^2$. Because of the small interaction cross-section, very large volume detectors are required to capture a sufficiently large sample of neutrinos to use for precision studies of their properties. For example, the interaction length of a neutrino with $E_\nu = 10\,\text{GeV}$ is of $\mathcal{O}(10^{10}\,\text{km})$.

Charged-current Quasi-elastic Scattering

Quasi-elastic scattering (QE)   with nucleons is the main process below $1\,\text{GeV}$. Protons are converted to neutrons in antineutrino interactions and vice-versa for neutrino interactions. Additionally, a charged lepton corresponding to the neutrino/antineutrino flavor is produced.

Resonant Scattering

Resonant scattering (RES)   describes the process of a neutrino scattering off a nucleon producing an excited state of the nucleon in addition to a charged lepton. RES is the leading process at 1.5-$5\,\text{GeV}$ for neutrinos and 1.5-$8\,\text{GeV}$ for antineutrinos.

Deep Inelastic Scattering

Deep inelastic scattering (DIS)   occurs if a neutrino carries sufficient energy to resolve the underlying structure of the nucleon and interacts with one of the composing quarks. DIS is the dominant process above $10\,\text{GeV}$. The nucleon breaks up and a lepton accompanied by a set of hadronic final states is produced. Whether the lepton is the charged lepton corresponding to the interacting neutrino type, or the neutrino itself depends on the type of DIS interaction. DIS happens via CC as in

$$\begin{aligned}
\nu_l + N &\rightarrow l^- + X, \\
\bar{\nu}_l + N &\rightarrow l^+ + X,
\end{aligned} \tag{2.1}$$

or NC interactions as

$$\nu_l + N \rightarrow \nu_l + X. \tag{2.2}$$

Here, X stands for any set of final state hadrons and N for the nucleon. The Feynman diagrams for the processes in Equations Equation 2.1 and Equation 2.2 are shown in Figure Figure 2.3.

Figure 2.3: Feynman diagrams for deep inelastic scattering of a neutrino with a nucleon via charged-current (left) and neutral current (right) interactions. Taken from [10].
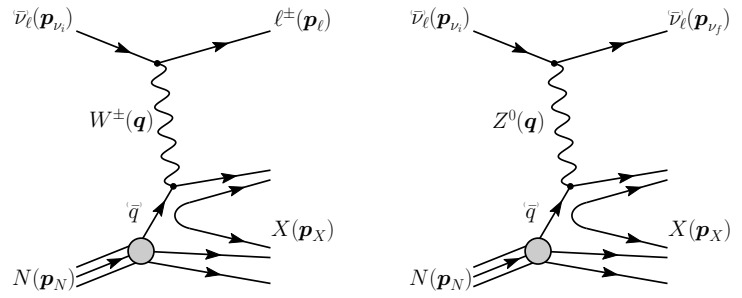
Beyond the Standard Model Neutrinos | 3

3.1 Neutrino Oscillations

3.1.1 Vacuum Oscillations

3.1.2 Oscillations in Matter

3.1.3 Atmospheric Neutrino Oscillations

Neutrino Production in the Atmosphere

The flux of neutrinos used for this work exclusively comes from the Earth's atmosphere. The nominal flux model is calculated by [12] in the energy range of 100 MeV to 10 TeV. When highly relativistic cosmic rays (protons and heavier nuclei [9]) interact in the upper atmosphere they produce a shower of particles. Neutrinos emerge from the decays of charged pions and kaons (π and K mesons) present in these showers. For energies below 100 GeV, the leading contribution comes from the pion decay chain

$$
\begin{aligned}
\pi^{\pm} &\rightarrow \mu^{\pm} + \nu_{\mu}(\bar{\nu}_{\mu}), \\
\mu^{\pm} &\rightarrow e^{\pm} + \bar{\nu}_{\mu}(\nu_{\mu}) + \nu_{e}(\bar{\nu}_{e}).
\end{aligned}
\tag{3.1}
$$

The muons that also originate from this process are considered the main background source for IceCube. The left part of Figure Figure 3.1 shows the atmospheric neutrino flux for the very broad energy spectrum in which they are produced. The flux expectations are calculated for the South Pole [12], where the IceCube detector is located. From Equation Equation 3.1 the ratio between muon and electron neutrinos can be inferred to be $N_{\nu_{\mu}} : N_{\nu_{e}} \approx 2 : 1$. This is only the case at muon energies below 1 GeV, where all muons decay in flight. For higher energies, muons can reach earth before decaying increasing the ratio to approximately 10:1 at around 100 GeV as shown in the right part of Figure Figure 3.1. Additionally, kaon decays start to contribute which also increases the number of muons and muon neutrinos.

In cosmic ray interactions, charged mesons or tau particles can also be produced, which leads to the formation of tau neutrinos. However, at the energy range considered for this work, the resulting tau neutrino flux is negligible as compared to the muon neutrino flux [13] and is not taken into account. It should be stated here that there is a rather large uncertainty on the normalization of the atmospheric neutrino flux on the order of 20-30 % [14] in the energy region of interest. This is mainly due to uncertainties in the primary cosmic ray spectrum and modeling of the hadronic interactions.

[12]: Honda et al. (2015), *Atmospheric neutrino flux calculation using the NRLMSISE-00 atmospheric model*

[9]: Tanabashi et al. (2018), *Review of Particle Physics*

[12]: Honda et al. (2015), *Atmospheric neutrino flux calculation using the NRLMSISE-00 atmospheric model*

[13]: Fedynitch et al. (2015), *Calculation of conventional and prompt lepton fluxes at very high energy*

[14]: Honda et al. (2007), *Calculation of atmospheric neutrino flux using the interaction model calibrated with atmospheric muon data*

Figure 3.1: Atmospheric neutrino fluxes of the different flavors as a function of energy (left) and ratios between muon- and electron-neutrinos as well as ratios between neutrinos and antineutrinos for both flavors (right). Calculations are done for the geographic South Pole. Taken from [12].
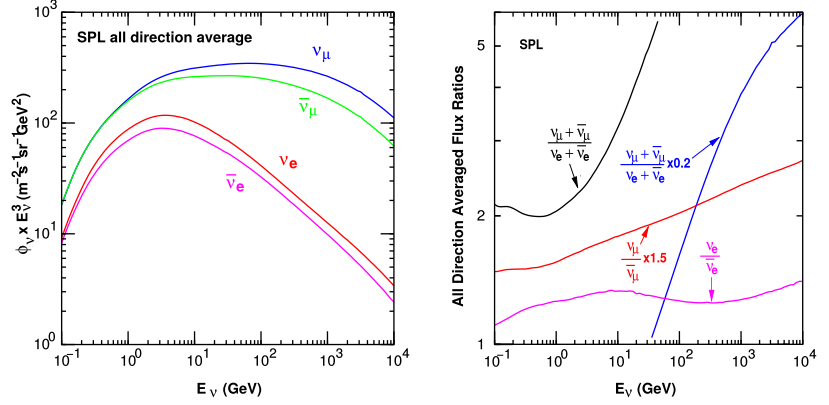
Oscillations of Atmospheric Neutrinos

[15]: Bilenky et al. (1978), *Lepton mixing and neutrino oscillations*

There are two ways to describe neutrino wave functions based on their Hamiltonian eigenvalues [15], as mass eigenstates or as flavor eigenstates. When applying a plane wave approach to explain the propagation of neutrinos in vacuum, their mass eigenstates evolve as

$$|\nu_k(t)\rangle = e^{-iE_k t/\hbar} |\nu_k\rangle \,, \tag{3.2}$$

where $E_k = \sqrt{\vec{p}^2 c^2 + m_k^2 c^4}$ is the energy of the mass eigenstate $|\nu_k\rangle$, with momentum $\vec{p}$ and mass m_k. Alternatively, they can be described in terms of their flavor eigenstates, which relate the neutrinos to the charged leptons they interact with in weak CC interactions. The flavor eigenstates are ν_e, ν_μ, and ν_τ, whereas the mass eigenstates are called ν_1, ν_2, and ν_3 in the standard three-neutrino model. To understand the propagation of distinct neutrino flavors in time (in vacuum) we need to relate the flavor eigenstates to the mass eigenstates. For massive neutrinos, each flavor eigenstate is a superposition of mass eigenstates [9]

[9]: Tanabashi et al. (2018), *Review of Particle Physics*

$$|\nu_\alpha\rangle = \sum_k U^*_{\alpha k} |\nu_k\rangle \,, \tag{3.3}$$

where $|\nu_\alpha\rangle$ are the weak flavor states with $\alpha = e, \mu, \tau$ and $|\nu_k\rangle$ the mass states with $k = 1, 2, 3$. $U_{\alpha k}$ is the Pontecorvo-Maki-Nakagawa-Sakata (PMNS) matrix defining the mixing between mass and flavor eigenstates. The mixing matrix can be parameterized as [9]

[9]: Tanabashi et al. (2018), *Review of Particle Physics*

$$U = \begin{pmatrix} 1 & 0 & 0 \\ 0 & c_{23} & s_{23} \\ 0 & -s_{23} & c_{23} \end{pmatrix} \begin{pmatrix} c_{13} & 0 & s_{13}e^{-i\delta_{CP}} \\ 0 & 1 & 0 \\ -s_{13}e^{i\delta_{CP}} & 0 & c_{13} \end{pmatrix} \begin{pmatrix} c_{12} & s_{12} & 0 \\ -s_{12} & c_{12} & 0 \\ 0 & 0 & 1 \end{pmatrix} \text{diag}(e^{i\rho_1}, e^{i\rho_2}, 1),$$
$$\tag{3.4}$$

where $c_{ij} = \cos\theta_{ij}$ and $s_{ij} = \sin\theta_{ij}$ are cosine and sine of the mixing angle θ_{ij}, that defines the strength of the mixing between the mass eigenstates i and j and δ_{CP} is the neutrino CP-violating phase. Nonzero, non-equal neutrino masses and the neutrino mixing relation in Equation Equation 3.3 lead to the observed phenomenon of neutrino oscillations. Oscillation means that a neutrino changes from its initial flavor to another flavor and back after traveling a certain distance. A produced flavor eigenstate $|\nu_\alpha\rangle$ propagates through space as a superposition of mass eigenstates. To find the probability that the initial flavor state $|\nu_\alpha\rangle$ ends up as the final

flavor state $|\nu_\beta\rangle$ after the time t we calculate

$$P_{\nu_\alpha \to \nu_\beta}(t) = |\langle \nu_\beta | \nu_\alpha(t) | \nu_\beta | \nu_\alpha(t)\rangle|^2, \tag{3.5}$$

where P is the probability calculated by applying Fermi's Golden Rule [16]. Fermi's Golden Rule explains the transition rate from one energy eigenstate to another depending on the strength of the coupling between the two. The strength of the coupling is described by the square of the matrix element. Using the unitarity of the mixing matrix $U^{-1} = U^\dagger$ to reverse the relation Equation 3.3 and then time evolve the mass eigenstates with Equation Equation 3.2 we get the time evolution of the flavor state $|\nu_\alpha(t)\rangle$. Inserting this result into Equation Equation 3.5 yields

$$P_{\nu_\alpha \to \nu_\beta}(t) = \sum_{j,k} U^*_{\beta j} U_{\alpha j} U_{\beta k} U^*_{\alpha k} e^{-i(E_k - E_j)t/\hbar}, \tag{3.6}$$

where the indices j and k run over the mass eigenstates. For small neutrino masses compared to their kinetic energy, we can approximate the energy as

$$E_k \approx E + \frac{c^4 m_k^2}{2E} \quad \longrightarrow \quad E_k - E_j \approx \frac{c^4 \Delta m_{kj}^2}{2E}, \tag{3.7}$$

where $\Delta m_{kj}^2 = m_k^2 - m_j^2$ is the mass-squared splitting between states k and j. If we now replace the time in Equation Equation 3.6 by the distance traveled by the relativistic neutrinos $t \approx L/c$ we get

$$
\begin{aligned}
P_{\nu_\alpha \to \nu_\beta}(t) = \delta_{\alpha\beta} &- 4 \sum_{j>k} \mathbf{Re}(U^*_{\beta j} U_{\alpha j} U_{\beta k} U^*_{\alpha k}) \sin^2\left(\frac{c^3 \Delta m_{kj}^2}{4E\hbar} L\right) \\
&+ 2 \sum_{j>k} \mathbf{Im}(U^*_{\beta j} U_{\alpha j} U_{\beta k} U^*_{\alpha k}) \sin^2\left(\frac{c^3 \Delta m_{kj}^2}{4E\hbar} L\right),
\end{aligned}
\tag{3.8}
$$

which is referred to as the survival probability if $\alpha = \beta$ and the transition probability if $\alpha \neq \beta$. The probability in Equation Equation 3.8 is only nonzero if there are neutrino mass eigenstates with masses greater than zero. Additionally, there must be a mass-squared difference Δm^2 and nonzero mixing between the states. Since we assumed propagation in vacuum in Equation Equation 3.2, the transition and survival probabilities correspond to vacuum mixing.

Matter Effects

3.2 Heavy Neutral Leptons

3.2.1 Motivation for Heavy Sterile Neutrinos

3.2.2 Extending the Standard Model

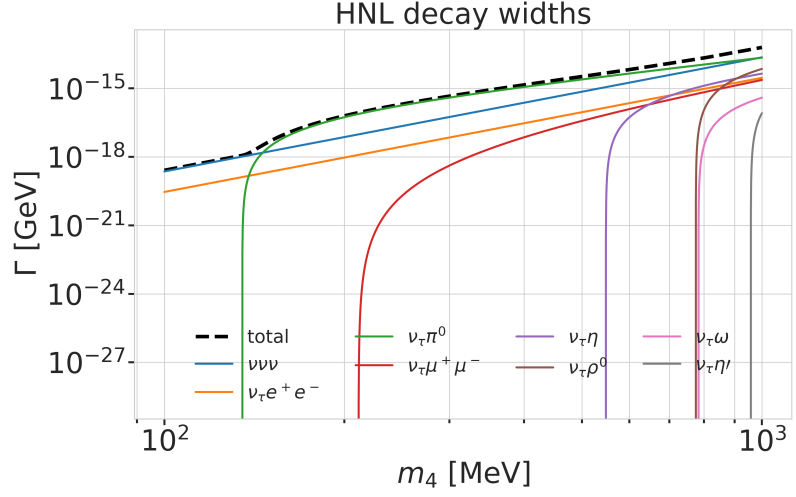### 3.2.3 Global Constraints on Mixing

Figure 3.2: Decay widths of the HNL within the mass range considered, calculated based on the results from [17]. Given the existing constraints on $|U_{e4}|^2$ and $|U_{\mu 4}|^2$, we consider that the corresponding decay modes are negligible.

3.3 Open Questions in Neutrino Particle Physics

The IceCube Neutrino Observatory | 4

This chapter explains the detection principle of the IceCube Neutrino Observatory as well as one of the reconstruction algorithms applied to extract information from the raw detector signals. Section 4.1 first presents the layout of IceCube and DeepCore before Section Section 4.2.1 and 4.2.2 explain the Cherenkov effect and the propagation of particles through ice. Finally, Section Section **??** outlines the reconstruction algorithm itself in detail.

(Re-)write IceCube chapter for PhD thesis (just copy paste from M.Sc.).

4.1 The IceCube In-Ice Array

(a) Schematic sketch

(b) Design and components of a DOM

Figure 4.1: The IceCube Neutrino Observatory and a schematic view of the Digital Optical Module (DOM). More detailed information can be found in [6].

[6]: Aartsen et al. (2017), *The IceCube Neutrino Observatory: instrumentation and online systems*

ABBASI2009294_data_acquisition
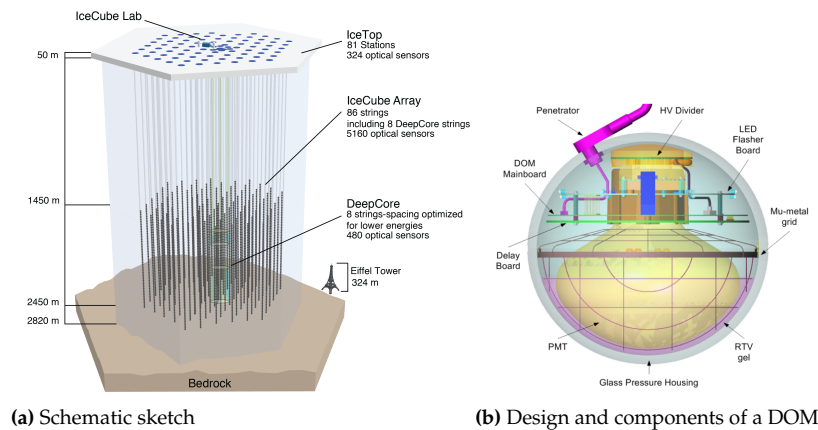
The IceCube Neutrino Observatory [6] is a cubic-kilometer particle detector located at the geographic south pole. The detector consists of 86 vertical strings with 5160 optical sensors called digital optical modules (DOMs) [**ABBASI2009294_data_acquisition**]. Figure **??** shows a schematic overview of the detector layout with its main components. The strings were drilled down into the Antarctic ice in a hexagonal arrangement shown in Figure Figure 4.2. 60 optical sensors are placed on each string at depths of 1450-2450 m below the ice. IceCube is designed to detect neutrinos in the energy range $\mathcal{O}$(GeV)-$\mathcal{O}$(PeV). Neutrinos can only be detected by the secondary charged particles created when they interact in the ice. The optical sensors detect Cherenkov light produced by these charged particles (see Section Section 4.2.1). Using the observed light pattern, the neutrino energy, direction, and flavor can be reconstructed as described in Section Section **??**. The DOMs are made of a spherical glass housing containing a 10 " photomultiplier tube (PMT) in addition to the readout and processing electronics. The modules are made to collect light, digitize the resulting PMT signal and send the data to the central data acquisition at the surface if a trigger condition is met. The design of a DOM and its components is shown in Figure Figure **??**.

The main part of IceCube is formed by 78 strings with 125 m horizontal spacing and 17 m vertical spacing between DOMs. This results in a neutrino detection energy threshold of 100 GeV. There are 8 additional

Figure 4.2: Top view of the IceCube array.

[18]: Abbasi et al. (2012), *The design and performance of IceCube DeepCore*

strings that form a denser sub-array of IceCube called DeepCore [18]. DeepCore is at the bottom-center of the detector and includes these 8 strings as well as the 7 surrounding IceCube strings in the fiducial volume shown in Figure Figure 4.2. The strings in this volume have an average distance of about 70 m. The majority of the DeepCore DOMs are placed between 2100 m and 2450 m below the ice and the vertical spacing is 7 m. Around 2050 m there is a dust layer with bad optical properties. Above the dust layer, there are a few additional DeepCore modules used as a veto cap. The denser spacing and the application of high quantum efficiency DOMs in DeepCore as well as the fact that the ice between 2100 m and 2450 m has the best optical properties leads to a lowered neutrino detection energy threshold of around 5 GeV. DeepCore is optimized for the observation of neutrinos in the energy range of $10 - 100$ GeV. This is the energy range where the oscillation signal from atmospheric neutrinos can be observed and studied. The surrounding IceCube strings and the veto cap are used to reject atmospheric muons that are the main background in neutrino oscillation measurements.

[6]: Aartsen et al. (2017), *The IceCube Neutrino Observatory: instrumentation and online systems*

The coordinate system [6] used in IceCube is centered at 46500'E, 52200'N at an elevation of 883.9 m. It is defined as a right-handed coordinate system with the y-axis pointing along the Prime Meridian (Grid North) towards Greenwich, UK and the x-axis pointing 90 degrees clockwise from the y-axis (Grid East). The z-axis is normal to the Earth's surface, pointing away from the surface. Additionally, the depth in IceCube is defined as the vertical distance from the ice surface, set to be at an elevation of 2832 m.

4.1.1 In-Ice Array

DeepCore

4.1.2 IceTop

4.1.3 Digital Optical Modules

4.2 Propagation of Particles in Ice

When charged particles travel through matter they interact and lose energy by several interaction processes. The Cherenkov light emitted by the particles as described in Section Section 4.2.1 only contributes a small amount to the total energy loss. The dominant processes depend on the type of Cherenkov light source, which we can broadly categorize into the three groups: quasi-continuous energy loss by muons, electromagnetic cascades, and hadronic cascades.

Muons lose their energy mainly by *ionization*, *bremsstrahlung*, *pair production* and the *photo-nuclear interaction*. Considering that ionization only has a weak energy dependence for muons above $1\,\text{GeV}$ and combining the other three components into one, the total energy loss is given by

$$-\frac{\mathrm{d}E}{\mathrm{d}x} = a_I(E) + b_R(E) \cdot E, \tag{4.1}$$

where E is the energy and $a_I(E)$ and $b_R(E) \cdot E$ are the energy loss by ionization and the combined radiative losses, respectively. For the energy range of interest for this work, the parameters $a_I(E)$ and $b_R(E)$ only have a weak energy dependence and equation Equation 4.1 reduces to

$$-\frac{\mathrm{d}E}{\mathrm{d}x} = a + b \cdot E. \tag{4.2}$$

This description results in a critical energy $E_{crit} = a/b$ separating the two energy regimes where ionization or radiative losses are dominant. Typical values are $a \approx 2.59\,\text{MeV/cm}$ and $b \approx 3.63 \cdot 10^{-6}\,\text{cm}^{-1}$ [**2004hep.ph....7075C**] leading to a critical energy of $\sim 770\,\text{GeV}$. Since the considered energy range for atmospheric neutrino oscillations is below the critical energy we only consider ionization losses by setting $b = 0$ which easily relates the range of a muon R_μ to its initial energy by

$$R = \frac{E_0}{a}. \tag{4.3}$$

With equation Equation 4.3 it is clear that by measuring the length of a muon track, its energy can be estimated if the full track is contained in IceCube. This treatment is only an approximation and does not take into account the stochastic nature of some of the energy losses. Especially bremsstrahlung and photo-nuclear interactions occur rarely, but when they happen, they deposit a large amount of energy. More detailed information is found in [19].

[19]: Raedel (2012), *Simulation Studies of the Cherenkov Light Yield from Relativistic Particles in High-Energy Neutrino Telescopes with Geant4*

4.2.1 Cherenkov Effect

Cherenkov radiation is emitted when a charged particle moves through a medium with a velocity that is greater than the speed of light in that medium. The continuous energy loss due to the emission of Cherenkov radiation is small, at the order of $\mathcal{O}(10^{-4})$, as compared to the main energy losses that will be described in Section Section 4.2.2. The observation of this radiation in IceCube and DeepCore, however, is fundamental for the detection of the charged particles originating from the neutrino interactions that were outlined in Section Section 2.3. The Cherenkov effect was first observed by Pavel Cherenkov in 1934 [20]. As can be derived from trigonometry, the Cherenkov light is emitted in a parallel wavefront at the Cherenkov angle

[20]: Cherenkov (1937), *Visible Radiation Produced by Electrons Moving in a Medium with Velocities Exceeding that of Light*

$$\theta_c = \arccos\left(\frac{1}{\beta n}\right), \tag{4.4}$$

with n being the refractive index of the medium and β the speed of the particle in units of the speed of light. A sketch of the wavefront is shown in Figure Figure 4.3, where the black circles depict spherically emitted light and the blue line is the formed Cherenkov light front. Typical values for
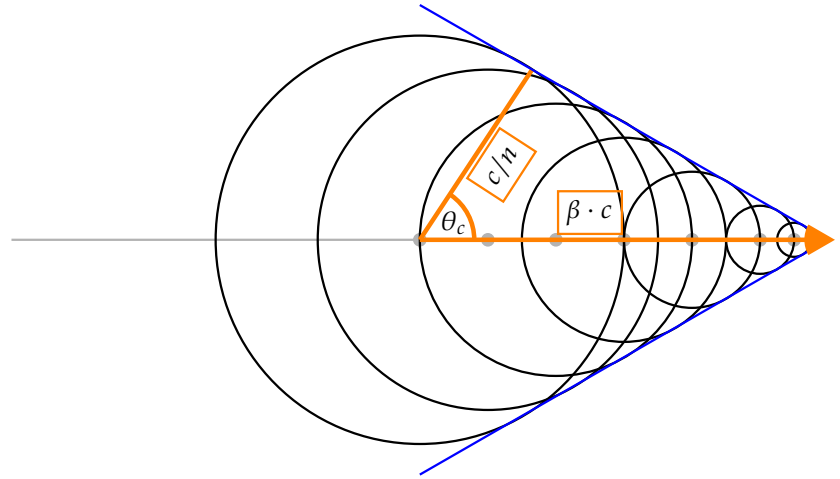
Figure 4.3: Schematic formation of the Cherenkov light front (blue) produced by a charged particle traveling faster than the speed of light in the medium. The black circles are spherically emitted light and the orange arrow shows the direction of the particle.

[21]: Euler (2014), *Observation of oscillations of atmospheric neutrinos with the Ice-Cube Neutrino Observatory*

Frank_Tamm

raedel_wiebusch_cherenkov_yield

the Antarctic ice are $n \approx 1.3$ and as a result $\theta_c \approx 41°$ [21]. Additionally, one can calculate the number of photons produced by a Cherenkov emitter based on the description in [**Frank_Tamm**]. For a wavelength λ with ($300\,\text{nm} < \lambda < 500\,\text{nm}$) 250 photons per cm are emitted assuming a very relativistic particle with $\beta \simeq 1$ [**raedel_wiebusch_cherenkov_yield**].

4.2.2 Energy Losses

Muons

Electromagnetic Showers

Electromagnetic cascades are induced by electrons and positrons or photons. All of them are either produced directly in the neutrino interactions or in interactions of secondary particles. Photons lose energy via pair production whereas for electrons and positrons the dominant energy loss is due to bremsstrahlung. For both cases, the interaction process

happens repeatedly and an electromagnetic shower is formed when pair production and bremsstrahlung take place in turn. Every time one of the interactions takes place, more electrons and positrons or photons are produced with smaller energy. This proceeds until the energy of the particles falls below the critical energy E_c and the remaining energy is quickly lost. For electrons and positrons, this happens through ionization and excitation of the surrounding atoms. For photons, the Compton effect and the photoelectric effect become the dominant energy losses. Electromagnetic showers are characterized by the radiation length X_0 at which the energy of electrons or positrons is reduced to $1/e$ of their initial energy. For photons, X_0 is 7/9 of the mean free path for pair production. For ice, the critical energy is $E_c \approx 78\,\text{MeV}$ and the radiation length is $X_0 \approx 39.3\,\text{cm}$ [9].

[9]: Tanabashi et al. (2018), *Review of Particle Physics*

Hadronic Showers

Hadronic cascades are always produced in the neutrino interactions described in Section Section 2.3, either from the breaking nucleus or as decay products. Similar to an electromagnetic cascade, a hadronic cascade forms as a result of the production of secondary particles from the strong interactions of hadrons with the traversed matter. Hadronic cascades also contain an electromagnetic component, for example through the decay of neutral pions into two photons. The shower profile and the light emission are very dependent on the produced particle type, which leads to larger fluctuations between individual showers with the same energy. The observed energy also varies, because energy gets lost in the hadronic binding process and muons and neutral particles produce less light and no light, respectively. On top of that, hadrons have a higher energy threshold for Cherenkov light production, due to their higher mass. The relative brightness of hadronic showers as compared to electromagnetic showers is given by [19]

[19]: Raedel (2012), *Simulation Studies of the Cherenkov Light Yield from Relativistic Particles in High-Energy Neutrino Telescopes with Geant4*

$$F(E) = \frac{T_{\text{hadron}}}{T_{\text{EM}}}, \tag{4.5}$$

where $T_{\text{hadron/EM}}$ is the total track length of a hadronic/electromagnetic shower with the same energy. The ratio $F(E)$ is always smaller than 1, but increases with energy as the electromagnetic fraction of the hadronic cascade becomes larger. A more detailed parameterization of $F(E)$, as well as fitted values for several particle types, can be found in [19].

[19]: Raedel (2012), *Simulation Studies of the Cherenkov Light Yield from Relativistic Particles in High-Energy Neutrino Telescopes with Geant4*

4.3 Particle Signatures in IceCube

4.3.1 Neutrinos

4.3.2 Atmospheric muons

Standard Model Background Simulation and Data Processing | 5

5.1 Event Generation

5.1.1 Neutrinos

5.1.2 Muons

5.2 Detector Simulation

5.2.1 Photon Propagation

5.2.2 Detector Respones

5.3 Processing

5.3.1 Trigger and Online Filter

5.3.2 Offline Filter

5.3.3 Hit Selection

To select hits that originated from direct photons, a procedure closely related to the one described in [22] is applied. The cleaning is based on removing hits from DOMs that could have originated from light emitted by any of the other hit DOMs on the same string. The selection solely uses the time of arrival (TOA) of the pulses. It is carried out for every detected event in the following steps:

[22]: Garza (2014), *Measurement of neutrino oscillations in atmospheric neutrinos with the IceCube DeepCore detector*

(i) Select strings where at least 3 DOMs have seen light.
(ii) Every hit DOM is characterized by the time of the earliest pulse (above a threshold of 0.1 photoelectron (PE)) and the integrated charge of all pulses.
(iii) For every string passing these criteria the following steps are performed:

  (a) Remove DOMs with hit outside of a time window of [-250 ns, +2000 ns] around the median TOA of all hits on the string.
  (b) Using the DOM with the highest charge as reference (estimate for point of closest approach), check if any of the other DOMs on the string lies in the time window

$$\left[t_r - \frac{d_{r,i}}{c_{\text{ice}}} - t_{\text{delay}}, t_r + \frac{d_{r,i}}{c_{\text{ice}}} + t_{\text{delay}} \right],$$ (5.1)

  where t_r is the TOA of the reference DOM, $d_{r,i}$ is the absolute distance between the two DOMs considered, c_{ice} is the speed of light in ice and t_{delay} is the allowed time delay. A time delay

of 20 ns is used to limit the selection to photons with little scattering.

(c) For each of the selected DOMs, it is now verified that, compared to each of the other selected DOMs, none was hit after the time $t_{\max}$

$$t_{\max} = t_i + \frac{d_{i,j}}{c_{\text{ice}}} + t_{\text{delay}}, \tag{5.2}$$

where the subscripts i and j stand for the two DOMs in questions, and all combinations are checked.

(d) As the last step, it is checked whether there are more than six empty modules between selected modules. Keeping the DOM with the largest charge, the other DOMs are checked going upwards and downwards along the string. Finally, only strings that still have three or more selected DOMs are kept and their hits are identified as direct pulses.

5.3.4 Reconstruction

There are several methods to select and reconstruct events in IceCube. At energies around 10-40 GeV, where we expect the oscillation signal, the events are faint and only a few DOMs detect light. One approach for the reconstruction of such events is described in this section. The reconstruction uses only photons that traveled along a straight line - called *direct* photons. Using direct photons has the benefit of reducing the systematic biases caused by the large variations of the bulk ice properties; scattering and absorption. With an average distance of 70 m between strings in DeepCore and an effective scattering length of about 50 m [23], there will always be a fraction of direct photons arriving at the DOMs. The used method applies a stepwise procedure, where first a cleaning routine selects events with direct photons as described in Section Section 5.3.3. Afterward, the direction of the particle is reconstructed and finally the energy is determined as outlined in Sections Section 5.3.4.

FLERCNN Event Reconstruction and Classification

Didn't copy over SANTA/LEERA since I need the FLERCNN desciption here.

Standard Model Event Topologies

The signals that IceCube detects vary depending on the neutrino flavor and interaction type of the event. The two main signatures that can be observed are track-like and cascade-like events. The observed Cherenkov light is produced by the secondary particles originating from the neutrino interactions described in Section Section 2.3. Table Table **??** shows an overview of the possible event signatures. Minimum ionizing muons can travel for long distances and are seen as extended light signatures called tracks. Muons can come from ν_μ-CC interactions or from ν_τ-CC followed by the decay of the τ to a muon. However, the τ only decays to a muon with a branching ratio of BR=17 %.

[23]: Lundberg et al. (2007), *Light tracking for glaciers and oceans: Scattering and absorption in heterogeneous media with Photonics*

Cascades are the light signal produced by the EM/hadronic showers described in Section Section 4.2.2. They come from ν_e-CC and most of the ν_τ-CC interactions because the electron and the tau lose all their energy quickly and only travel a short distance. They are also produced in all ν-NC interactions since only the hadronic shower is observable and the produced neutrino escapes unseen. The cascades at the energies considered in this work have a smaller radius than the spacing of the DOMs and are therefore seen as point-like light emitters.

The existence of the two types of event topologies and their origins imply that by identifying track-like events we can identify events coming (mainly) from ν_μ-CC interactions and therefore obtain a flavor identification. This is a crucial part of performing an oscillation analysis as will be further discussed in Section Section 8.1.

5.4 Systematic Uncertainties

5.4.1 Detector Property Variations

5.4.2 Atmospheric Flux

Heavy Neutral Lepton Signal Simulation | 6

6.1 Model Independent Simulation

6.1.1 Generator Functions

6.1.2 Simplistic Sets

6.1.3 Realistic Set

6.2 Model Specific Simulation

Re-write/re-formulate this section (copied from HNL technote).

6.2.1 Custom LeptonInjector

Signal events are simulated using a custom LeptonInjector (LI) tool [24], modified from its standard version to include the HNL particle and the description of the HNL decays needed to produce the double cascade signature (currently only ν_τ related). In its SM work mode, LI injects a lepton and a cascade (under the general name *Hadrons*) at the interaction vertex of the neutrino. Both objects have the same (x,y,z,t) coordinates. In the modified version, the lepton at the interaction vertex is replaced by the HNL. After a chosen distance the HNL is forced to decay. The decay is sampled from the kinematically accessible decay modes shown in Figure 6.2.

[24]: Abbasi et al. (2021), *LeptonInjector and LeptonWeighter: A neutrino event generator and weighter for neutrino observatories*

A big addition to the standard LI is that the decay products of the HNL are added to the list of particles in the I3MCTree with a displaced position and delayed time from the interaction vertex. These daughter particles form a second cascade, not in the form of a *Hadrons* object, but as the explicit particles forming the shower. The kinematics of the two-body decays are computed analytically, while the three-body decays are dealt with using MadGraph5. To do so, we randomly pick an event from a list that we generated for each three-body decay mode. Independent of the number of particles in the final state of the HNL decay, the kinematics are calculated/simulated at rest and then boosted along the HNL momentum. The decay mode is randomly chosen based on the mass dependent branching ratios shown in Figure 6.2.

Each file is produced by running the generation level processing script using the filenumber as random seed and the above settings for the sampling distributions. The main part is calling the *MultiLeptonInjector* module in *volume mode* adding two generators (for ν_τ and $\bar{\nu}_\tau$) with 50% of the events. The generators are provided with the custom double-differential/total cross section splines described in Section 6.2.1 and the parameters defining the sampling distributions. For each frame *OneWeight* and a reference weight are also calculated and stored using the weighting functions and a baseline atmospheric ν_τ flux + oscillation spline. The weight will later be calculated inside of the analysis framework

Figure 6.1: Custom HNL total cross sections for the four target masses compared to the total ($\nu_\tau / \bar{\nu}_\tau$ neutral current) cross section used for SM neutrino simulation production with GENIE.
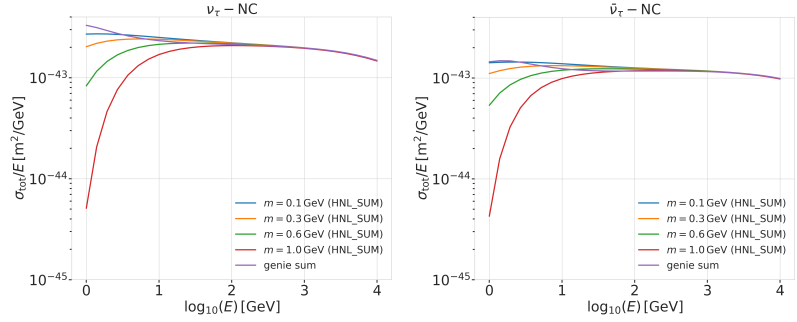
PISA, based on the input OneWeight. In addition to the i3 file itself, a LeptonInjector configuration file is written which stores the needed information to produce event weights using LeptonWeighter. Optionally the script can also produce an hdf5 file with the same name in the same location. This will store a fixed set of keys, extracted from the i3 file.

We are using *volume mode,* for the injection of the primary particle on a cylindrical volume. The main generation/sampling happens in `VolumeLeptonInjector::DAQ` inside `LeptonInjector.cxx`. After writing the config (s) frame (currently not kept), the energy is sampled from a power law distribution, then the cosine(zenith) and azimuth angles are sampled from uniform distributions. The (x,y) position is sampled uniform in r, ϕ (for position on disk) and the z position is sampled from a uniform distribution. After the primary properties have been sampled the *EventProperties* is created and handed over to the `FillTree` functions which is where the custom HNL simulation happens:

Cross Sections

The cross sections are calculated using a modified version of Carlos Argüelles' NuXSSplMkr, which is a tool to calculate neutrino cross sections from parton distribution functions (PDFs) and then produce splines that can be read and used with IceCube software. The main modification to calculate the cross sections for the ν_τ neutral current interaction into the new heavy mass state is the addition of a kinematic condition to ensure that there is sufficent energy to produce the heavy mass state. It is the same confition that needs to be fulfilled for the charged current case, where the outgoing lepton mass is non-zero. Following [25] (equation 7), the condition

$$(1 + x\delta_N)h^2 - (x + \delta_4)h + x\delta_4 \leq 0, \tag{6.1}$$

is implemented for the neutral current case. Here $\delta_4 = \frac{m_4^2}{s - M^2}$, $\delta_N = \frac{M^2}{s - M^2}$, and $h \stackrel{def}{=} xy + \delta_4$, with x, y being the Bjorken variables, m_4 and M the mass of the heavy state and the target nucleon, respectively, and s the center of mass energy squared. Since the (SM) neutrino background simulation used for this analysis was created using GENIE (version 2.12.8), interfaced through the IceCube software package *genie-icetray*, with the GRV98LO PDFs, those were added as *GRV98lo_patched* to the cross section spline maker, to ensure the best possibe agreement. Double-differential ($ds\,dx\,dy$) and total (σ) cross sections were produced for the

[25]: Levy (2009), *Cross-section and polarization of neutrino-produced tau's made simple*
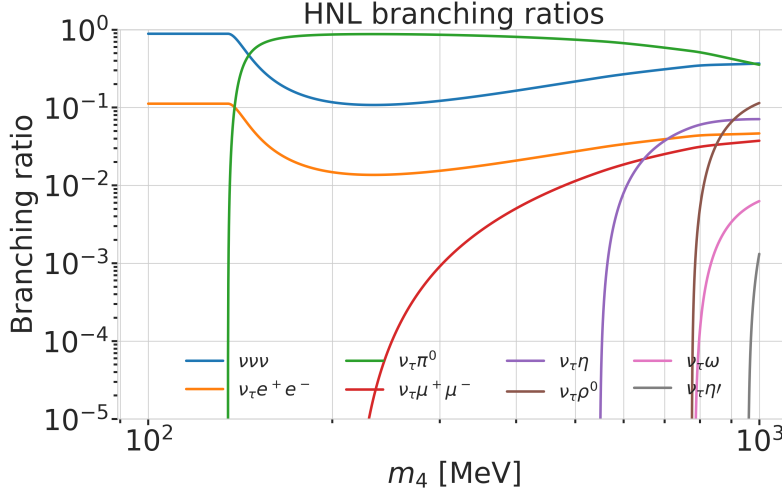
Figure 6.2: Branching ratios of the HNL within the mass range considered, calculated based on the results from [17]. Given the existing constraints on $|U_{e4}|^2$ and $|U_{\mu4}|^2$, we consider that the corresponding decay modes are negligible.

Table 6.1: xx

Channel	Opens [MeV]	Max BR [%]
$\nu_4 \to \nu_\tau \nu_\alpha \bar{\nu}_\alpha$	0	100.0
$\nu_4 \to \nu_\tau e^+ e^-$	1	?
$\nu_4 \to \nu_\tau \pi^0$	135	?
$\nu_4 \to \nu_\tau \mu^+ \mu^-$	211	?
$\nu_4 \to \nu_\tau \eta$	548	?
$\nu_4 \to \nu_\tau \rho^0$	770	?
$\nu_4 \to \nu_\tau \omega$	783	?
$\nu_4 \to \nu_\tau \eta'$	958	?

four target HNL masses and then splined. The produced cross section splines are stored in the resources of the custom LeptonInjector module. Figure 6.1 shows the total cross sections that were produced compared to the cross section used for the production of the SM $\nu_\tau / \bar{\nu}_\tau$ neutral current background simulation .

> Add comparions of SM cross sections between NuXSS-plMkr and genie

Decay Channels

The accessible decay channels are dependent on the mass of the HNL and the allowed mixing. For this analysis, where only $|U_{\tau4}|^2 \neq 0$, the considered decay channels are listed in Table 6.1 and the corresponding branching ratios are shown in Figure 6.2. The indiviudal branching ratio for a specific mass is calculated as $\mathrm{BR}_i(m_4) = \Gamma_i(m_4)/\Gamma_{\text{total}}(m_4)$, where $\Gamma_{\text{total}}(m_4) = \sum \Gamma_i(m_4)$. The formulas to calculate the decay width show up in multiple references, but we chose to match them to [17], which also discusses the discrepencies in previous literature.

[17]: Coloma et al. (2021), *GeV-scale neutrinos: interactions with mesons and DUNE sensitivity*

2-Body Decay Widths The decay to a neutral pseudoscalar mesons is

$$\Gamma_{\nu_4 \to \nu_\tau P} = |U_{\tau4}|^2 \frac{G_F^2 m_4^3}{32\pi} f_P^2 (1 - x_p^2)^2, \qquad (6.2)$$

with $x_P = m_P/m_4$ and

$$f_{\pi^0} = 0.130 \,\text{GeV}, \qquad f_\eta = 0.0816 \,\text{GeV}, \qquad C_2 = f_{\eta'} = -0.0946 \,\text{GeV}, \qquad (6.3)$$

while the decay to a neutral vector meson is given by

$$\Gamma_{\nu_4 \to \nu_\tau V} = |U_{\tau 4}|^2 \frac{G_F^2 m_4^3}{32\pi} \left(\frac{f_V}{m_V}\right)^2 g_V^2 (1 + 2x_V^2)(1 - x_V^2)^2, \quad (6.4)$$

with $x_V = m_V / m_4$,

$$f_{\rho^0} = 0.171\,\text{GeV}^2, \qquad f_\omega = 0.155\,\text{GeV}^2, \quad (6.5)$$

and

$$g_{\rho^0} = 1 - 2\sin^2\theta_w, \qquad g_\omega = \frac{-2\sin^2\theta_w}{3}, \qquad \sin^2\theta_w = 0.2229 \quad (6.6)$$

[26]: Tiesinga et al. (2021), *CODATA recommended values of the fundamental physical constants: 2018*

[26].

3-Body Decay Widths   The (invisible) decay to three neutrinos is

$$\Gamma_{\nu_4 \to \nu_\tau \nu_\alpha \bar{\nu_\alpha}} = |U_{\tau 4}|^2 \frac{G_F^2 m_4^5}{192\pi^3}, \quad (6.7)$$

while the decay to two charged leptons (using $x_\alpha = (m_\alpha/m_4)^2$) of the same flavor reads

$$\Gamma_{\nu_4 \to \nu_\tau l_\alpha^+ l_\alpha^-} = |U_{\tau 4}|^2 \frac{G_F^2 m_4^5}{192\pi^3} \left[C_1 f_1(x_\alpha) + C_2 f_2(x_\alpha)\right], \quad (6.8)$$

with the constants defined as

$$C_1 = \frac{1}{4}(1 - 4s_w^2 + 8s_w^4), \qquad C_2 = \frac{1}{2}(-s_w^2 + 2s_w^4), \quad (6.9)$$

the functions as

$$f_1(x_\alpha) = (1 - 14x_\alpha - 2x_\alpha^2 - 12x_\alpha^3)\sqrt{1 - 4x_\alpha} + 12x_\alpha^2(x_\alpha^2 - 1)L(x_\alpha), \quad (6.10)$$

$$f_2(x_\alpha) = 4[x_\alpha(2 + 10x_\alpha - 12x_\alpha^2)\sqrt{1 - 4x_\alpha} + 6x_\alpha^2(1 - 2x_\alpha + 2x_\alpha^2)L(x_\alpha)], \quad (6.11)$$

and

$$L(x) = \ln\left(\frac{1 - 3x_\alpha - (1 - x_\alpha)\sqrt{1 - 4x_\alpha}}{x_\alpha(1 + \sqrt{1 - 4x_\alpha})}\right). \quad (6.12)$$

6.2.2 MadGraph5 3-Body Decays

[17]: Coloma et al. (2021), *GeV-scale neutrinos: interactions with mesons and DUNE sensitivity*

The code to produce the 3-body decay kinematics is MadGraph4 v3.4.0 based on the decay diagrams calculated with FeynRules 2.0 using the Lagrangians derived in [17]. The Universal FeynRules Outpur (UFO) from `effective_HeavyN_Majorana_v103` were used for our calculation. For each meass and corresponding decay channel, we produce $1e06$ decay kinematic variations (rest frame) and store those in a text file.

variable	distribution	range
energy	E^{-2}	$[2, 10^4]$ GeV
zenith	uniform (in $\cos(\theta)$)	$[180\,°, 80\,°]$
azimuth	uniform	$[0\,°, 360\,°]$
vertex (x, y)	uniform	$r = 600$ m
vertex z	uniform	$[-600, 0]$ m
m_{HNL}	fixed	$[0.3, 0.6, 1.0]$ GeV
L_{decay}	L^{-1}	$[0.0004, 1000.0]$ m / $[1.0, 1000.0]$ m

Table 6.2: Sampling distributions of HNL simulation generation.

6.2.3 Sampling Distributions

This is the description of the signal simulation generator used to (re-)start simulation production in December 2023. The underlying sampling distributions are listed in Table 6.2. Judging from how the generation/processing efficiency was for the 190607 set, we target $1e04$ files per set with $5e05$ events per file at generation, resulting in a maximum of $5e09$ events per set at generation level. Note here that the actual number of events per set at generation might be a little lower since some events won't be allowed if they don't have enough energy to produce the HNL.

6.2.4 Weighting Scheme

The weighting for the HNL signal simulation happens in a custom stage of PISA. The only input is the stored OneWeight and the variable physics parameter $|U_{\tau 4}|^2$, which is the mixing strength of the new heavy mass state and the tau sector. The custom re-weighting is needed to go from the used sampling PDF ($1/L$ with fixed range in lab frame decay length) to the target PDF (exponential defined by proper lifetime of the HNL). For each event the re-weighting factor is calculated using the gamma factor

$$\gamma = \frac{\sqrt{E_{\mathrm{kin}}^2 + m_{\mathrm{HNL}}^2}}{m_{\mathrm{HNL}}}, \tag{6.13}$$

with the HNL mass m_{HNL} and it's kinetic energy E_{kin}. The speed of the HNL is calculated as

$$v = c \cdot \sqrt{1 - \frac{1}{\gamma^2}}, \tag{6.14}$$

where c is the speed of light. With these the lab frame decay length range can be converted into the rest frame lifetime range for each event

$$\tau_{\mathrm{min/max}} = \frac{s_{\mathrm{min/max}}}{v \cdot \gamma}. \tag{6.15}$$

The proper lifetime of each HNL event can be calculated using the total decay width Γ_{total} shown in Figure 3.2 and the chosen mixing strength $|U_{\tau 4}|^2$ as

$$\tau_{\mathrm{proper}} = \frac{\hbar}{\Gamma_{\mathrm{total}}(m_{\mathrm{HNL}}) \cdot |U_{\tau 4}|^2}, \tag{6.16}$$

where $\hbar$ is the reduced Planck constant. Since the decay length/lifetime of the events is sampled from an inverse distribution instead of an exponential as it would be expected from a particle decay we have to re-weight accordingly to achieve the correct decay length/lifetime

distribution. This is done by using the wanted exponential distribution

$$\text{PDF}_{\text{exp}} = \frac{1}{\tau_{\text{proper}}} \cdot e^{\frac{-\tau}{\tau_{\text{proper}}}},\tag{6.17}$$

and the inverse distribution that was sampled from

$$\text{PDF}_{\text{inv}} = \frac{1}{\tau \cdot (\ln(\tau_{\text{max}}) - \ln(\tau_{\text{min}}))}.\tag{6.18}$$

The lifetime re-weighting factor is calculated as

$$w_{\text{lifetime}} = \frac{\text{PDF}_{\text{exp}}}{\text{PDF}_{\text{inv}}} = \frac{\Gamma_{\text{total}}(m_{\text{HNL}}) \cdot |U_{\tau 4}|^2}{\hbar} \cdot \tau \cdot (\ln(\tau_{\text{max}}) - \ln(\tau_{\text{min}})) \cdot e^{\frac{-\tau}{\tau_{\text{proper}}}}.\tag{6.19}$$

Adding another factor of $|U_{\tau 4}|^2$ to account for the mixing at the interaction vertex the total re-weighting factor becomes

$$w_{\text{total}} = |U_{\tau 4}|^2 \cdot w_{\text{lifetime}},\tag{6.20}$$

which can be applied on top of flux and oscillation weight to get the final HNL weight for a given mixing (and mass).

Detecting Low Energetic Double Cascades | 7

7.1 xx

7.1.1 xx

Search for an Excess of Heavy Neutral Lepton Events

8

8.1 Statistical Analysis

8.1.1 Test Statistic

8.1.2 Free Parameter Selection

8.1.3 Signal and Background in Analysis Binning

8.2 Modelling of Detector Response via Likelihood-Free Inference

8.3 Analysis Checks

8.3.1 Minimzer Stability

8.3.2 Ensemble Tests

8.3.3 Background Only Three-Flavor Oscillation Measurement

8.3.4 Heavy Neutral Lepton Sensitivity

8.4 Results

8.4.1 Best Fit Parameters

8.4.2 Upper Limits

8.4.3 Post-Fit Data/MC Agreement

Summary and Outlook | 9

9.1 Summary

9.1.1 Three-Flavor Oscillation Measurement

9.1.2 Heavy Neutral Lepton Search

Double Cascade Sensitivity

Shape Excess Search

9.2 Outlook

9.2.1 Shape Analysis Improvements

- ▶ estimate full contribution from cascade only events (underestimated due to limited sampling distributions)
- ▶ include double cascade classifier into Binning
- ▶ further optimize binning

9.2.2 Test Coupling to Electron/Muon Flavor

9.2.3 IceCube Upgrade

Conclusion | 10

10.1 Conclusion

APPENDIX

A

First Appendix

Bibliography

Here are the references in citation order.

[1] W. Pauli. "Dear radioactive ladies and gentlemen". In: *Phys. Today* 31N9 (1978), p. 27 (cited on page 1).

[2] C. L. Cowan et al. "Detection of the Free Neutrino: a Confirmation". In: *Science* 124.3212 (1956), pp. 103–104. DOI: 10.1126/science.124.3212.103 (cited on page 1).

[3] G. Danby et al. "Observation of High-Energy Neutrino Reactions and the Existence of Two Kinds of Neutrinos". In: *Phys. Rev. Lett.* 9 (1 July 1962), pp. 36–44. DOI: 10.1103/PhysRevLett.9.36 (cited on page 1).

[4] K. Kodama et al. "Observation of tau neutrino interactions". In: *Physics Letters B* 504.3 (2001), pp. 218–224. DOI: https://doi.org/10.1016/S0370-2693(01)00307-0 (cited on page 1).

[5] R. Davis et al. *Proceedings of the Neutrino '72 Europhysics Conference*. Vol. 1. Baltonfuered, Hungary, 1972, p. 29 (cited on page 1).

[6] M. G. Aartsen et al. "The IceCube Neutrino Observatory: instrumentation and online systems". In: *Journal of Instrumentation* 12.3 (Mar. 2017), P03012. DOI: 10.1088/1748-0221/12/03/P03012 (cited on pages 1, 11, 12).

[7] Mark Thomson. *Modern particle physics*. Cambridge [u.a.]: Cambridge University Press, 2013, XVI, 554 S. (Cited on pages 3, 4).

[8] Sheldon L. Glashow. "Partial-symmetries of weak interactions". In: *Nuclear Physics* 22.4 (1961), pp. 579–588. DOI: https://doi.org/10.1016/0029-5582(61)90469-2 (cited on page 3).

[9] M. Tanabashi et al. "Review of Particle Physics". In: *Phys. Rev. D* 98 (3 Aug. 2018), p. 030001. DOI: 10.1103/PhysRevD.98.030001 (cited on pages 3, 4, 7, 8, 15).

[10] Andrii Terliuk. "Measurement of atmospheric neutrino oscillations and search for sterile neutrino mixing with IceCube DeepCore". PhD thesis. Berlin, Germany: Humboldt-Universität zu Berlin, Mathematisch-Naturwissenschaftliche Fakultät, 2018. DOI: 10.18452/19304 (cited on pages 4, 6).

[11] J. A. Formaggio and G. P. Zeller. "From eV to EeV: Neutrino cross sections across energy scales". In: *Rev. Mod. Phys.* 84 (3 Sept. 2012), pp. 1307–1341. DOI: 10.1103/RevModPhys.84.1307 (cited on page 4).

[12] M. Honda et al. "Atmospheric neutrino flux calculation using the NRLMSISE-00 atmospheric model". In: *Phys. Rev. D* 92 (2 July 2015), p. 023004. DOI: 10.1103/PhysRevD.92.023004 (cited on pages 7, 8).

[13] Anatoli Fedynitch et al. "Calculation of conventional and prompt lepton fluxes at very high energy". In: *European Physical Journal Web of Conferences*. Vol. 99. European Physical Journal Web of Conferences. Aug. 2015, p. 08001. DOI: 10.1051/epjconf/20159908001 (cited on page 7).

[14] M. Honda et al. "Calculation of atmospheric neutrino flux using the interaction model calibrated with atmospheric muon data". In: *Phys. Rev. D* 75 (4 Feb. 2007), p. 043006. DOI: 10.1103/PhysRevD.75.043006 (cited on page 7).

[15] S.M. Bilenky and B. Pontecorvo. "Lepton mixing and neutrino oscillations". In: *Physics Reports* 41.4 (1978), pp. 225–261. DOI: 10.1016/0370-1573(78)90095-9 (cited on page 8).

[16] P. A. M. Dirac. "The Quantum Theory of the Emission and Absorption of Radiation". In: *Proceedings of the Royal Society of London Series A* 114.767 (Mar. 1927), pp. 243–265. DOI: 10.1098/rspa.1927.0039 (cited on page 9).

[17] Pilar Coloma et al. "GeV-scale neutrinos: interactions with mesons and DUNE sensitivity". In: *Eur. Phys. J. C* 81.1 (2021), p. 78. DOI: 10.1140/epjc/s10052-021-08861-y (cited on pages 10, 23, 24).

[18] R. Abbasi et al. "The design and performance of IceCube DeepCore". In: *Astropart. Phys.* 35.10 (2012), pp. 615–624. DOI: 10.1016/j.astroparthys.2012.01.004 (cited on page 12).

[19] Leif Raedel. "Simulation Studies of the Cherenkov Light Yield from Relativistic Particles in High-Energy Neutrino Telescopes with Geant4". MA thesis. Aachen, Germany: Rheinisch-Westfälischen Technischen Hochschule, 2012 (cited on pages 13, 15).

[20] P. A. Cherenkov. "Visible Radiation Produced by Electrons Moving in a Medium with Velocities Exceeding that of Light". In: *Phys. Rev.* 52 (4 Aug. 1937), pp. 378–379. DOI: 10.1103/PhysRev.52.378 (cited on page 14).

[21] Sebastian Euler. "Observation of oscillations of atmospheric neutrinos with the IceCube Neutrino Observatory". PhD thesis. Aachen, Germany: Rheinisch-Westfälischen Technischen Hochschule, 2014 (cited on page 14).

[22] Juan Pablo Yáñez Garza. "Measurement of neutrino oscillations in atmospheric neutrinos with the IceCube DeepCore detector". PhD thesis. Berlin, Germany: Humboldt-Universität zu Berlin, Mathematisch-Naturwissenschaftliche Fakultät I, 2014. DOI: 10.18452/17016 (cited on page 17).

[23] Johan Lundberg et al. "Light tracking for glaciers and oceans: Scattering and absorption in heterogeneous media with Photonics". In: *Nucl. Instrum. Meth.* A581 (2007), pp. 619–631. DOI: 10.1016/j.nima.2007.07.143 (cited on page 18).

[24] R. Abbasi et al. "LeptonInjector and LeptonWeighter: A neutrino event generator and weighter for neutrino observatories". In: *Comput. Phys. Commun.* 266 (2021), p. 108018. DOI: 10.1016/j.cpc.2021.108018 (cited on page 21).

[25] Jean-Michel Levy. "Cross-section and polarization of neutrino-produced tau's made simple". In: *J. Phys. G* 36 (2009), p. 055002. DOI: 10.1088/0954-3899/36/5/055002 (cited on page 22).

[26] Eite Tiesinga et al. "CODATA recommended values of the fundamental physical constants: 2018". In: *Rev. Mod. Phys.* 93 (2 June 2021), p. 025010. DOI: 10.1103/RevModPhys.93.025010 (cited on page 24).

Acknowledgements

Who to thank for this mess?!